Kinetic and Thermodynamic Aspects in the Microwave-Assisted Synthesis of ZnO Nanoparticles in Benzyl Alcohol

Idalia Bilecka, Pierre Elser, and Markus Niederberger*

Laboratory for Multifunctional Materials, Department of Materials, ETH Zürich, Wolfgang-Pauli-Strasse 10, 8093 Zürich, Switzerland

ABSTRACT A detailed study of kinetic and thermodynamic aspects in the microwave-assisted synthesis of ZnO nanoparticles from zinc acetate and benzyl alcohol is presented. The use of a nonaqueous sol—gel approach provides the unique opportunity to investigate simultaneously the organic reaction, that is, the esterification between acetate and benzyl alcohol, and the inorganic process, represented by the growth of the ZnO nanoparticles. Monitoring both the formation of the organic species as well as ZnO crystal size with time makes it possible to directly correlate the kinetics of the organic side reaction with the growth kinetics of the ZnO nanoparticles. The esterification reaction, which is the chemical basis for producing the monomers for ZnO formation, was found to be first order. The growth of the ZnO nanoparticles followed the Lifshitz—Slyozov—Wagner model for coarsening, pointing to a diffusion-limited process. Comparison of the microwave-mediated route with conventional heating showed that microwave irradiation greatly accelerates nanoparticle formation by (a) facilitating the dissolution of the precursor in the solvent, (b) increasing the rate constants for the esterification reaction by 1 order of magnitude, resulting in faster production of monomer and consequently in an earlier nucleation event, and (c) increasing the rate constants k_{growth} for the crystal growth from 3.9 nm^3/min (conventional heating) to 15.4 nm^3/min (microwave heating).

KEYWORDS: benzyl alcohol · kinetics of nanoparticle formation · metal oxides · microwave chemistry · nanoparticles · nonaqueous sol–gel synthesis · zinc oxide

The possibility to tune the physical and chemical properties of nanoscale materials through varying the crystal size and shape is the major driving force in nanoparticle research, providing new opportunities for many technological applications.[1−3] However, this fascinating effect also brings an additional challenge to the synthetic chemist, because in addition to being able to control the composition of a product, its morphological characteristics have to be manipulated in an, ideally, rational and predicted fashion. Colloidal nonhydrolytic liquid-phase routes have been applied with great success to the size- and shape-controlled synthesis of semiconductor nanoparticles in general,[3−5] but also for metal oxide nanostructures in particular.[6,7] In comparison to these well-established approaches, the use of microwave irradiation represents a relatively new strategy in nanoparticle synthesis.[8−12] But the rapidly growing number of publications reporting microwave-assisted routes to all kinds of inorganic nanoparticles ranging from metals[13,14] to oxides,[15−28] chalcogenides,[29−37] and phosphates[38,39] gives a strong indication of their great capability and versatility. In organic chemistry, microwave irradiation has been applied for decades as a powerful heating tool, leading to short reaction times and improved yields.[40,41] The particularity of microwave heating is the volumetric nature of the power dissipation in a dielectric, which causes heating directly inside the sample.[41] This *in situ* mode of energy conversion leads to a fast heating rate with minimized thermal gradients, thus offering perfect conditions for an efficient synthesis of inorganic nanoparticles. The actual knowledge about the influence of microwave irradiation on metal oxide synthesis[42] proposes that (i) the fast heating increases the net rate early in the process, (ii) the suppressed heating of the reaction vessel minimizes the problem of inhomogeneities caused by thermal gradients, resulting in a more uniform reaction, while generating a rapid and intense heating, (iii) the surface of oxides is covered by microwave-absorbing hydroxyl groups, thus changing the surface temperature and producing local overheating.[27,42,43]

In nonaqueous sol—gel routes to metal oxide nanoparticles, organic reaction pathways play a crucial role.[44] Parallel to the formation of the inorganic nanoparticles, the initial organic species (*i.e.*, solvent and organic constituent of the precursor) undergo chemical reactions that are responsible for supplying the oxygen for the metal oxide, but also strongly influence particle size, shape, surface/assembly properties and, in

*Address correspondence to markus.niederberger@mat.ethz.ch.

Received for review December 8, 2008 and accepted January 27, 2009.

Published online February 24, 2009.
10.1021/nn800842b CCC: $40.75

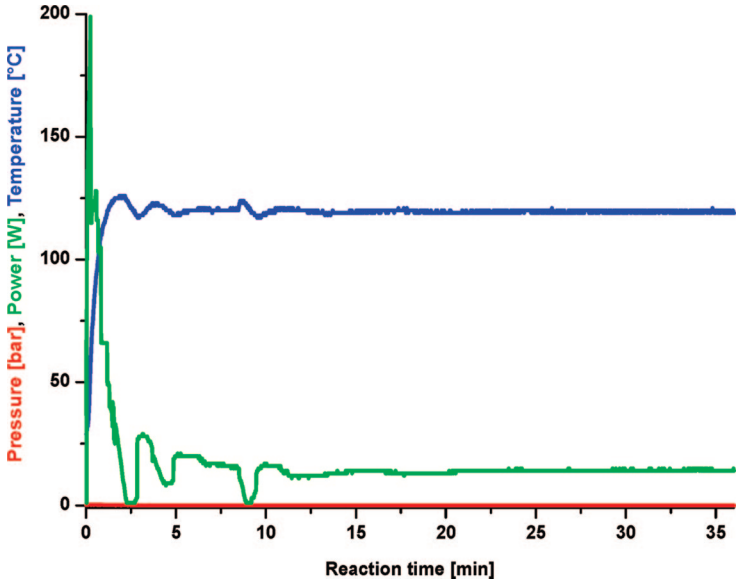

Figure 1. Temperature, pressure, and output power profile during microwave heating at 120 °C.

selected cases, even composition and crystal structure. The high sensitivity of organic reactions toward microwave irradiation makes it obvious to combine nonaqueous sol−gel with microwave chemistry, thus potentially providing a way to control the formation of inorganic nanoparticles through influencing the organic reaction pathways. Results in this direction have already been published for the preparation of various metal oxide nanoparticles such as ZnO, Fe_3O_4, CoO, MnO, and $BaTiO_3$.[27,45]

Although nanoparticle research made immense progress in the past few years, the development of rational synthesis strategies remains one of the major challenges. Only a detailed knowledge about nanoparticle formation, including not only chemical and crystallization mechanisms, but also thermodynamic and kinetic aspects, will make it possible to prepare a targeted compound in a predicted way. In the case of nonaqueous sol−gel chemistry, nanoparticle formation was up-to-now mainly described by the chemistry (reactivity and concentration of the chemical species involved) and by thermodynamic parameters like temperature and, to a lesser extent, pressure. The chemistry is clearly dominated by organic reaction pathways, leading to the situation that the reactivity of the precursor-solvent system has to be carefully adjusted to obtain crystalline metal oxide nanoparticles with the desired composition. However, in addition to these parameters, also the study of kinetic aspects is required, involving time-dependent analysis and quantification of both the organic species and the inorganic solid present in the liquid phase. It is obvious that a detailed knowledge of the growth mechanism and the various rate constants represent the basis for controlling the particle size, for optimizing the synthesis protocol, and for developing a rational synthesis planning.

The study of growth mechanism and formation kinetics of particles has a long tradition in colloid chemistry (see for example the work by La Mer,[46,47] Reiss,[48] Nielsen,[49] or Sugimoto[50]), and more recently nanoparticles renewed the interest of understanding the growth process in liquid phase.[51−53] Especially II−VI (CdS, CdSe) and III−V (InP, InAs) semiconductor quantum dots due to their size dependent luminescent properties allowed mechanistic studies by the use of optical absorption spectroscopy or photoluminescence.[54,55] In this context, Peng *et al.* described crystal size focusing and defocusing and how the crystal growth can be opitimized by adjusting the monomer concentration.[56] Other systematic studies were performed on transition metal oxide nanoparticles. A kinetic study of the formation of iron oxide demonstrated that both "heating up" and "hot injection" could be explained by the same theoretical framework based on the La Mer model.[57] Zinc oxide has been investigated in great detail by the group of Searson *et al.*,[58−62] but also by others,[63,64] taking into account the effect of organic ligands, solvent, and reactant concentrations. Other kinetic studies were performed on tungstates,[20] MoO_3,[65] TiO_2,[66] or SnO_2.[67] However, growth kinetics under microwave irradiation has hardly been investigated. Examples in this direction include enhanced oriented attachment processes in the case of Gd-doped ceria,[22] or the influence of microwave frequency on the particle morphology of $BaTiO_3$.[28]

In this manuscript we highlight kinetic and thermodynamic aspects in the microwave-mediated, nonaqueous sol−gel synthesis of ZnO, including a comparison between microwave and conventional heating, to find out why microwave-mediated approaches are so fast. The growth of the ZnO nanocrystals has been analyzed by using isothermal kinetic analyses. The combination of IR spectroscopy as quantification method for the organic monomeric species in solution with X-ray diffraction for following the crystal growth makes it possible to simultaneously monitor the organic and inorganic pathways. A series of experiments was performed to elucidate the crystal growth mechanism and to study the influence of several parameters such as concentration, temperature, and heating mode. We show that the crystal size in microwave-assisted nonaqueous sol−gel routes is dependent on both the organic reaction as well as on the crystal growth mainly due to coarsening. Acceleration of the reaction under microwave irradiation was observed to be due to improved dissolution of the precursor and faster kinetics of both the organic esterification reaction and the inorganic crystal growth. The kinetic and thermodynamic data gained from these experiments sets the basis for a better understanding of nanoparticle growth, which can directly be used for the controlled adjustment of the crystal size. On the

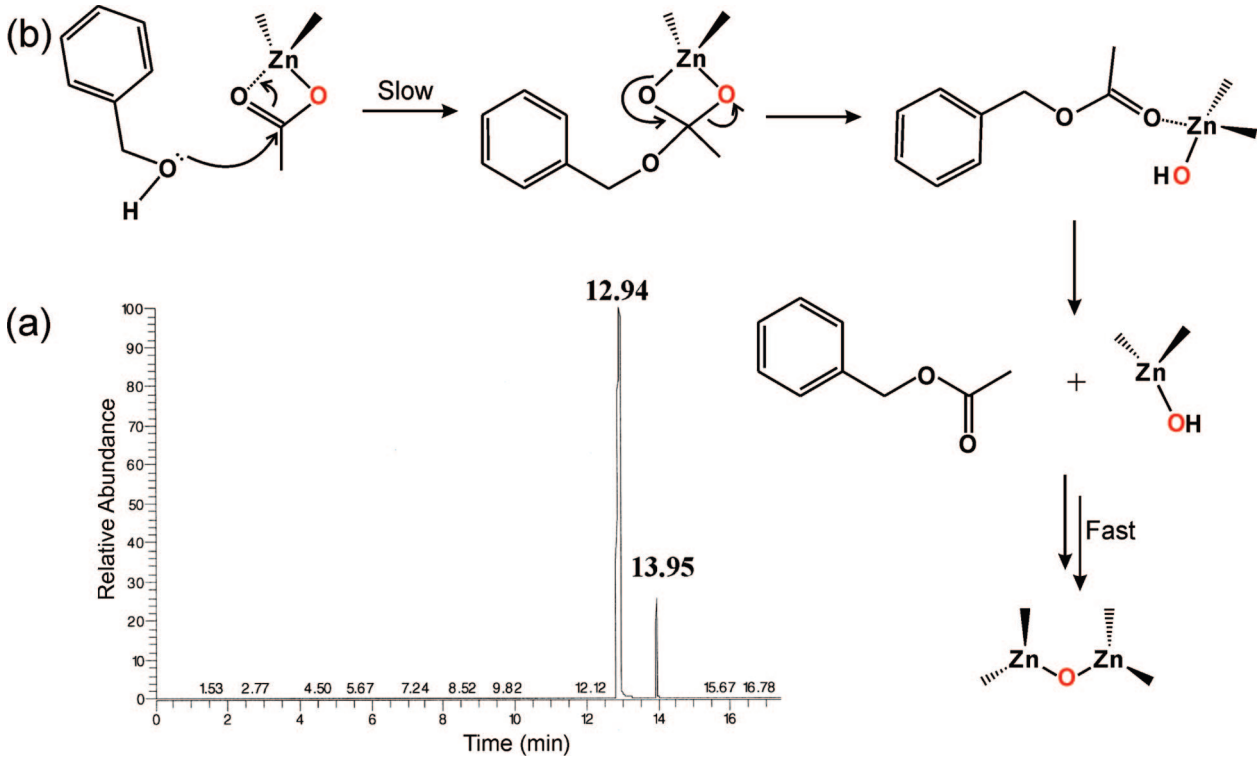

Figure 2. (a) Gas chromatogram of the final organic reaction solution with two elution peaks at 12.94 and 13.95 min corresponding to benzyl alcohol and benzyl acetate, respectively. (b) Ester elimination reaction as a result of a nucleophilic attack of benzyl alcohol on zinc acetate, finally resulting in the formation of benzyl acetate and zinc oxide.

longer term, however, these findings represent an important step toward the development of generally valid concepts for a rational and predictable synthesis planning.

RESULTS AND DISCUSSION

The formation of inorganic nanoparticles in solution involves the two processes nucleation and growth. Both the nucleation and growth greatly affect the particle size, size distribution, and morphology. According to classical theory, nucleation as a key step is induced by supersaturation conditions in the reaction solution. The peculiarity of nonaqueous sol−gel chemistry is that the supersaturation results from an organic reaction; that is, the monomers, defined as the chemical subunits contributing to crystal growth by condensation onto or dissolving from the nanoparticle surface, are provided by an organic reaction. The strong relation between the inorganic polymerization and the organic condensation reaction in nonaqueous sol−gel chemistry makes it necessary to discuss both pathways in the same context. The formation of ZnO can be divided into several sequential steps: (I) precursor solvation, (II) monomer formation by an esterification reaction, (III) nucleation, and (IV) crystal growth:

$$P_{solid} \overset{k_{solvation}}{\rightleftharpoons} P_{dissolved} \overset{k_{esterification}}{\rightleftharpoons} M_{dissolved} \overset{k_{nucleation}}{\rightleftharpoons}$$

$$M_{n(solid)} \overset{k_{growth}}{\rightleftharpoons} M_{n+m(solid)}$$

P is the precursor, M is the monomer, and $k_{solvation}$, $k_{esterification}$, $k_{nucleation}$, and k_{growth} are the rate constants for zinc acetate solvation, ester elimination reaction, nucleation, and growth, respectively. Thermodynamically, the growth of nanoparticles can be described as a sequence of thermodynamic barriers composed of four successive transition states separated by $E_a^{solvation}$, $E_a^{esterification}$, $E_a^{nucleation}$, and E_a^{growth}, representing the activation energy for precursor solvation, monomer formation, nucleation, and growth, respectively.

In the case of ZnO nanoparticle formation, the first step consists of the dissolution of zinc acetate in benzyl alcohol, which initiates the monomer formation through an ester elimination reaction between the acetate molecule and benzyl alcohol. Benzyl alcohol as solvent and reactant is present in large excess, so that the reaction can be considered as pseudo-first-order:

$$\frac{d[Zn(II)Ac]}{dt} = -k_{esterification}[Zn(II)Ac]$$

The relationship between the rate constant of the esterification reaction $k_{esterification}$ and the temperature is given by the Arrhenius equation:

$$k_{esterification} = Ae\left(\frac{-E_a^{esterification}}{RT}\right)$$

where A represents the pre-exponential factor, $E_a^{esterification}$ is the activation energy, T is the

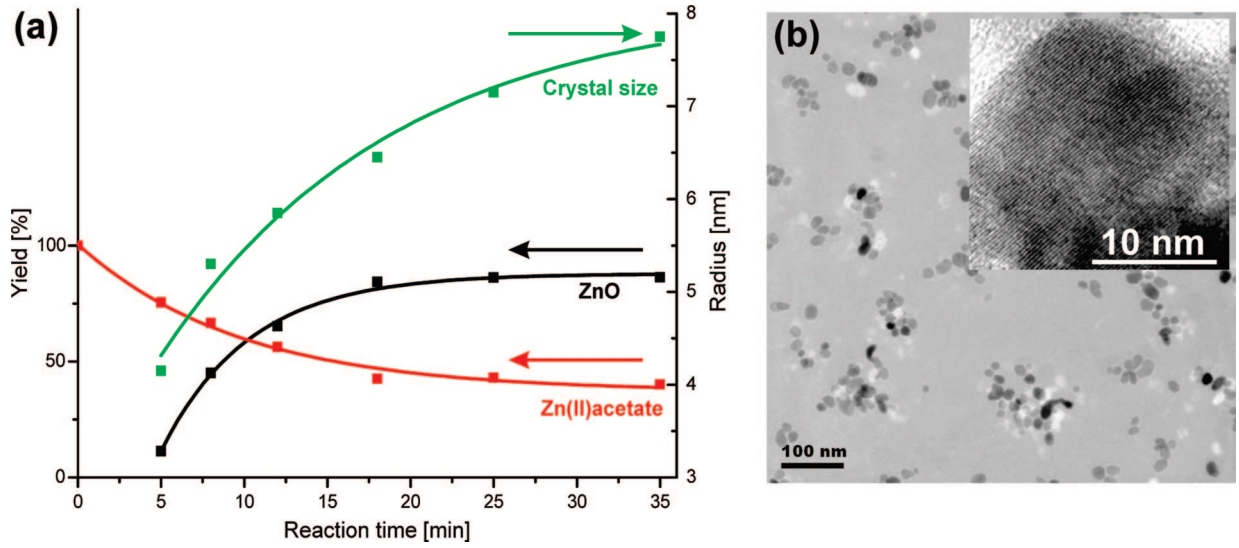

Figure 3. (a) Time-dependent evolution of the crystal size (green curve), yield of ZnO powder (black curve), and zinc acetate concentration (red curve) at 120 °C. (b) TEM overview image of ZnO nanoparticles obtained at 120 °C after 3 min (inset: HRTEM image of one particle).

reaction temperature, and R is the ideal gas constant.

The crystal growth process can be discussed in an analogous way to the esterficiation reaction. Because nucleation and growth are in the case of ZnO dominated by coarsening effects (Ostwald ripening),[60] that is, growth of larger crystals at the expense of smaller ones, the mathematical approach developed by Lifshitz−Slyozov−Wagner (LSW) can be applied. The LSW theory describes a diffusion limited growth behavior, in which either mass transport or reaction at the interface is the rate-limiting step.[68,69] The modified LSW theory, taking additionally the volume fraction of the precipitate into account,[70] provides the rate law for diffusion limited coarsening $r^3 - r_o^3 = k_{growth}t$, predicting that the average particle size cubed is proportional to the time t (r_o is the average initial particle radius at $t = 0$). By plotting r^3 against t a linear dependency, with the slope corresponding to k_{growth}, should be found in the case of diffusion controlled particle coarsening. Further details about Ostwald ripening theory and (modified) LSW theory can be found elsewhere.[71]

Microwave heating in combination with nonaqueous sol−gel chemistry provides a perfect model system for the investigation of nanoparticle formation in liquid phase. On the one hand, it is possible to influence the organic reactions occurring in parallel to nanoparticle formation by applying microwave irradiation, and on the other hand, these organic reactions can easily be understood on the basis of simple organic chemistry principles. In this work, we studied the growth of zinc oxide nanoparticles using isothermal kinetic analysis. IR spectroscopy was used for the quantification of benzyl acetate as organic product of the ester elimination process, and XRD was used for following the evolution of crystal size. The correlation of benzyl acetate formation with XRD data makes it possible to directly connect the kinetics of the organic side reaction with the growth kinetics of the ZnO nanoparticles. The ZnO nanoparticles were prepared by reacting zinc(II) acetate with benzyl alcohol in the microwave at temperatures ranging from 120 to 180 °C. Additionally, ZnO syntheses were carried out at 120 °C in a conventional laboratory oil bath (without using microwave irradiation) under otherwise identical reaction conditions. Comparison of these two heating procedures makes it possible to draw some general conclusions regarding the effect of microwave irradiation on the formation of ZnO nanoparticles. It is important to note that all the syntheses described in here resulted in the same and only products, namely ZnO nanoparticles with the zincite structure on the inorganic side, and benzyl acetate on the organic side.

The synthesis in the microwave oven was performed with a microwave irradiation source consisting of a magnetron tube operating at 2.45 GHz with a power output that can be varied between 0 and 300 W. The solutions were rapidly stirred by a magnetic stir bar to ensure high homogeneity. To prevent thermal gradients the reactions were carried out in 5 mL tubes. The temperature profile consists of thermal ramping, heating at the set-point and thermal quenching. Figure 1 shows a typical temperature, pressure, and output power profile for a reaction at 120 °C, demonstrating a rapid heating-up period of 1.2 min to the set point of 120 ± 4 °C. Then, the reaction is cooled down to room temperature by a compressed air flow within 1 min. The heating up and cooling down periods were kept identical for all samples.

The chemical composition of the reaction solutions after removal of the ZnO precipitate was determined by GC−MS (Figure 2a). Independent of the re-

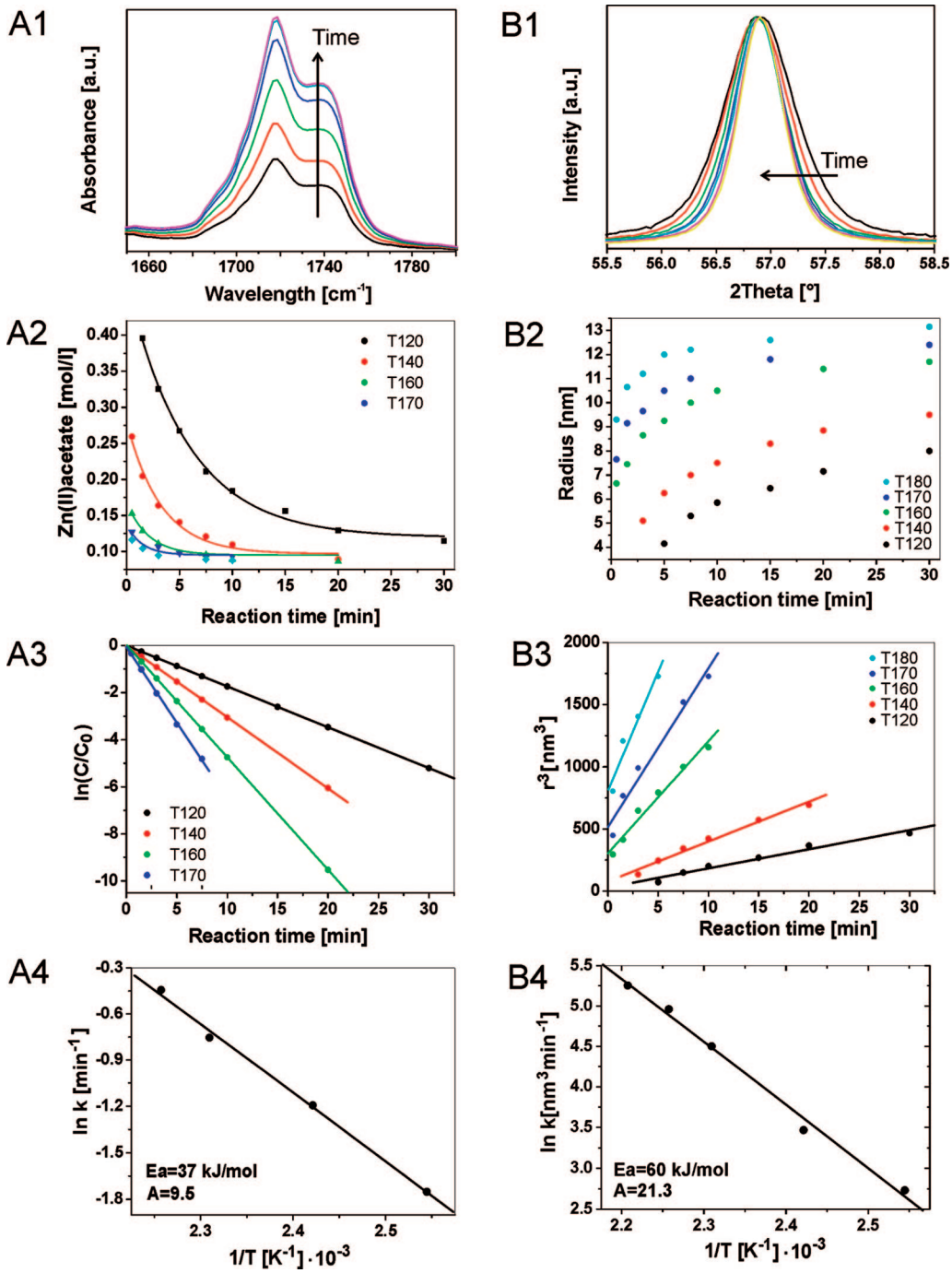

Figure 4. (Panels A) Benzyl acetate formation: (A1) FTIR spectra of the carbonyl bands of benzyl acetate after different reaction times; (A2) zinc(II) acetate concentration *vs* reaction time for different temperatures, fitted to an integrated first-order rate law; (A3) plot of ln(C/C_0) *vs* time for benzyl acetate formation for different temperatures; (A4) Arrhenius plot ln $k_{esterification}$ *vs* 1/*T*. (Panels B) ZnO crystal growth: (B1) Evolution of the normalized (110) reflection of the XRD pattern of the zincite nanopowder with time at 160 °C; (B2) plot of the ZnO crystal size *vs* reaction time; (B3) crystal radius r^3 *vs* reaction time; (B4) Arrhenius plot for the coarsening process.

action temperature and heating mode, only benzyl alcohol (elution peak at 12.94 min) and benzyl acetate (elution peak at 13.95 min) were detected. The presence of benzyl acetate clearly proves that the formation of the ZnO nanoparticles involves an ester elimination mechanism (Figure 2b), in agreement with previous reports.[45,72] The intensity of the benzyl acetate peak, and thus the benzyl acetate concentration, increased with extending the reaction time.

Figure 3a nicely illustrates the relation between the yield of formed ZnO powder (black curve), crystal size (green curve), and zinc acetate concentration (red curve) at 120 °C for different irradiation times. FTIR spectroscopy was used to quantify the benzyl acetate concentration in solution, and from this value the remain-

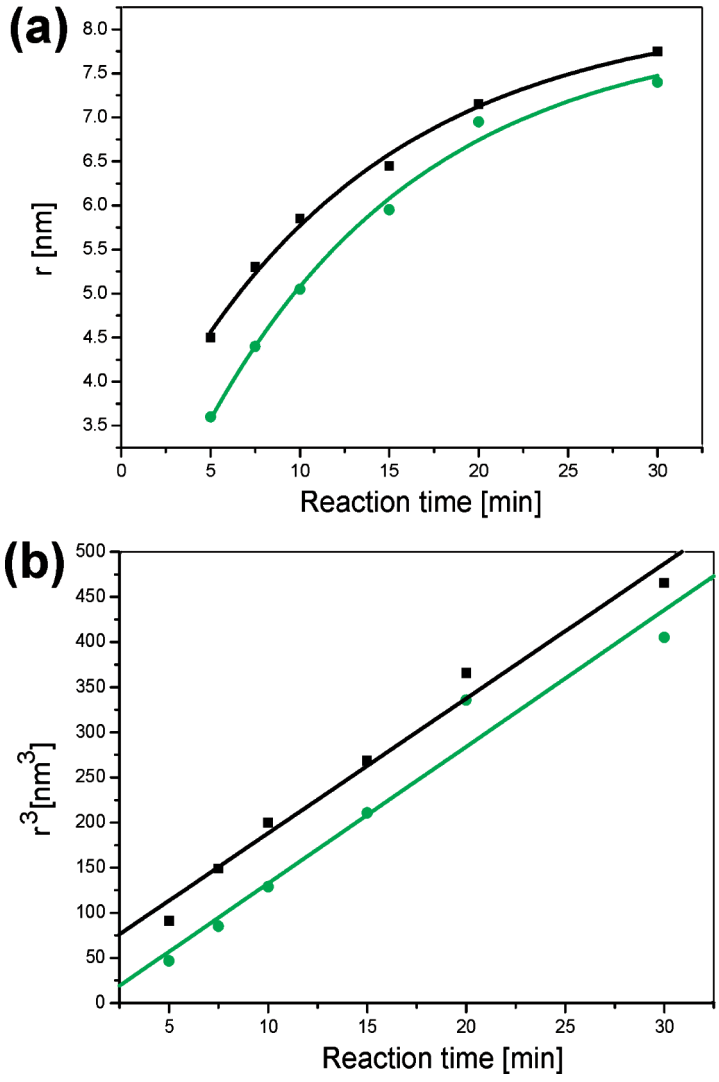

Figure 5. Effect of precursor concentration (green, 0.5 M; black, 1.5 M) at 120 °C on (a) ZnO crystal size *vs* time, (b) crystal radius cubed *vs* time.

ing zinc acetate was calculated. The spectra show, due to the polar environment caused by the solvent benzyl alcohol,[73] two well-defined bands at 1740 and 1717 nm (see below), which can be assigned to the C═O vibration of the ester, and which do not overlap by any of the benzyl alcohol absorption peaks. The yield was simply determined by weighing the precipitated powder. The crystal size was extracted from the (110) reflection in the XRD pattern by Scherrer analysis. It takes about 5 min of irradiation time at 120 °C to obtain phase-pure ZnO nanoparticles with crystal sizes of 8−9 nm (Figure 3a, green curve). Precipitates collected before were not phase pure and contained considerable amounts of zinc acetate. Between 5 and 35 min of irradiation time, the crystal size grows continuously to 15−16 nm, and zinc acetate is consumed due to the esterification reaction occurring parallel to ZnO formation. Its concentration drops from the initial concentration C_0 (C_0 = 100%, defined as the residual concentration of zinc acetate after the thermal ramping step) to about 35−40% within 18 min, from when on it remains constant (Figure 3a, red curve). The yield of ZnO increases with time, but reaches a maximum value of about 80% after about 18 min and then also remains constant. A closer look at the three curves reveals some expected, but nevertheless remarkable correlations between the three parameters crystal size, synthesis yield, and zinc acetate concentration. The fact that nanocrystalline ZnO particles are formed only after about 5 min of microwave irradiation, when approximately 25% of the zinc acetate is already transformed into benzyl acetate, underlines the importance of the esterification reaction for producing the monomers required for ZnO nucleation. Comparison of the yield with the zinc acetate concentration shows an inversely related behavior with comparable kinetics. With decreasing zinc acetate concentration, the ZnO yield increases and both values become constant after 18 min; that is, the system reaches a dynamic equilibrium between the dissolved monomer molecules and the solid metal oxide. Interestingly, the crystal size still increases with irradiation time, indicating that Ostwald ripening becomes the only growth mode for longer reaction times.

Figure 3b shows a TEM overview image of the ZnO nanoparticles synthesized at 120 °C, together with a HRTEM image of one ZnO nanoparticle as inset. The particle diameters range from 10 to 25 nm, which agrees well with the *XRD* data. The HRTEM image proves the single crystalline nature of the particles.

The esterification reaction of the acetate molecules with benzyl alcohol to benzyl acetate represents, as mentioned before, the chemical basis for the generation of the ZnO nanoparticles. Because the organic reaction pathway is inseparably connected to nanoparticle formation, kinetic data for the organic reaction is also highly relevant for the ZnO system. The relationship between the organic esterification reaction with the inorganic crystal growth is graphically summarized in Figure 4, presenting the organic and inorganic data next to each other. The four panels on the left-hand side (A) refer to the organic side, whereas the four panels on the right-hand side (B) illustrate the inorganic part.

First, we will discuss the time dependence of the esterification reaction (panels A). The esterification plays a crucial role for the nucleation and growth kinetics of the ZnO nanoparticles. The quantity of the reactive monomeric species is directly related to the benzyl acetate concentration; that is, by measuring the benzyl acetate concentration in solution with time, one gets an estimation of how much reactive monomer is available for ZnO formation. The change of the benzyl acetate concentration with reaction time was monitored by FTIR, recording the carbonyl vibration of the ester in the range of 1650 to 1800 cm^{-1}. As an example, Figure 4 A1 shows the time dependence of the carbonyl bands at 120 °C. The intensity of the bands, and thus the concentration of benzyl acetate, increases with increasing

reaction time. The kinetic study was done by performing the synthesis at 120, 140, 160, 170, and 180 °C, respectively, under otherwise similar conditions. The corresponding concentration profiles for zinc acetate are plotted in Figure 4A2. The initial ramping stage complicates the kinetic analysis, because isothermal conditions are not possible at the beginning of the reaction. Therefore, the initial zinc acetate concentration C_0 is defined as the one obtained after the thermal ramping step, and only the isothermal part of the reaction is considered. For this reason, the starting concentrations are different for the different temperatures. At higher reaction temperatures, most of the zinc acetate is already consumed after the ramping due to faster reaction rates. The benzyl acetate concentrations decrease exponentially, as expected for a first order reaction, until reaching a nearly constant value of about 0.1 mol/L after 20 min for all temperatures except for 120 °C, which takes longer than 30 min to reach the minimum.

On the basis of the integrated rate law $\ln(C/C_0) = (-k_{\text{esterification}}t)$, $\ln(C/C_0)$ is plotted against the reaction time at different temperatures in Figure 4A3. Linear regression with a deviation of less than 2% confirms the first-order rate law and thus allows the determination of the rate constants $k_{\text{esterification}}$ for different temperatures directly from the slopes of the straight lines. The as-obtained kinetic values, summarized in Table 1, range from 0.173 to 0.682 min^{-1}, increasing with temperature. It should also be mentioned that the precursor is only poorly soluble in benzyl alcohol, and therefore the contribution of the dissolution of zinc acetate cannot be neglected. Even though no detailed kinetic study was performed on the dissolution process, it could be observed that at 120 °C zinc acetate is completely dissolved after 3 min of microwave irradiation. Consequently, the observed reaction rates for benzyl acetate formation are a combination of precursor dissolution and esterification rates.

The temperature dependence of the rate constants follows the Arrhenius equation. Figure 4A4 shows a plot of the natural logarithm of the rate constants $k_{\text{esterification}}$ *versus* the inverse temperature. The activation energy $E_a^{\text{esterification}}$ can be calculated from the slope (divided by R) of the Arrhenius diagram and amounts to about 37 kJ/mol. The pre-exponential factor A, found at the intercept, is 9.5.

Now we will have a closer look at the time and temperature dependence of the inorganic crystal growth (panels B). The evolution of the crystal size can easily be followed by the peak broadening in the *XRD* pattern. Figure 4B1 shows the change in peak broadening of the (110) reflection of ZnO nanopowders obtained at 160 °C after different reaction times, clearly proving a narrowing of the reflection, and thus a growing crystal size, with reaction time. Figure 4B2 plots the obtained crystal sizes for the different reaction temperatures *versus* time, giving evidence that the crystal sizes increase with reaction time and with temperature. After 10 min of irradiation, for example, the crystal size is roughly 11 nm at 120 °C, 14 nm at 140 °C, and 20 nm at 160 °C; that is, the crystal growth is faster at higher temperatures. On the other hand, Figure 4B2 also shows that the growth rate of the ZnO nanoparticles is initially fast, but slows down with increasing crystal size. The LSW plot in Figure 4B3 results, as a matter of fact, in a linear dependence of the radius cubed on the reaction time. This relationship strongly supports a growth model for ZnO based on the LSW theory for coarsening; that is, the crystal growth occurs by a diffusion-limited process. The rate constants k_{growth} can directly be determined from the slopes of these straight lines, varying from 15.4 $\text{nm}^3\ \text{min}^{-1}$ at 120 °C to 191.8 $\text{nm}^3\ \text{min}^{-1}$ at 180 °C. The complete set of values is summarized in Table 1. The temperature dependence of the growth rate constants also follows the Arrhenius equation (Figure 4B4). Linear regression performed on the data in Figure 4B4 results in $\ln k_{\text{growth}} = 21.3 - 60/T$, which means that the activation energy is 60 kJ mol^{-1} and the pre-exponential factor A is 21.3.

In addition to the reaction temperature and time, also the effect of different concentrations was studied at 120 °C. At this low temperature, the ramping effect on lowering the precursor concentration during heating-up is the smallest. Figure 5a shows the average crystal size *versus* time at two different precursor concentrations, 0.5 M (green curve) and 1.5 M (black curve). In both cases, the size increases with aging time; however, larger crystals are formed at higher concentrations. A plot of r^3 *versus* time based on the LSW analysis (Figure 5b) proves that change of concentration does neither affect the linearity nor the slope of the lines, which means that the rate constant for coarsening is independent of the initial precursor concentration.

Comparison of the kinetic and thermodynamic data from our experiments (see also Table 1) with literature results shows that the activation energy of 37 kJ/mol for benzyl acetate formation in our system is close to the values of 30−45 kJ/mol, which were reported for zeolite-catalyzed esterification reactions of benzyl alcohol with acetic acid (activation energy without catalyst:

TABLE 1. Summary of the Data Obtained for the Growth of ZnO Nanocrystals from Zinc Acetate in Benzyl Alcohol Involving an Ester Elimination Reaction Using Microwave and Conventional Heating

		ester elimination		crystal growth	
heating mode	temperature [K]	yield [%]	$k_{\text{ester.}}$ [min^{-1}]	$r_{(t=10\text{min})}$ [nm]	k_{growth} [$\text{nm}^3 \cdot \text{min}^{-1}$]
microwave	393	71	0.173	5.8	15.36
	413	77	0.306	7.5	32.08
	433	78	0.477	10.5	90.19
	443	77	0.682	11.5	142.71
	453			12.2	191.81
conventional	395		0.0142		3.9

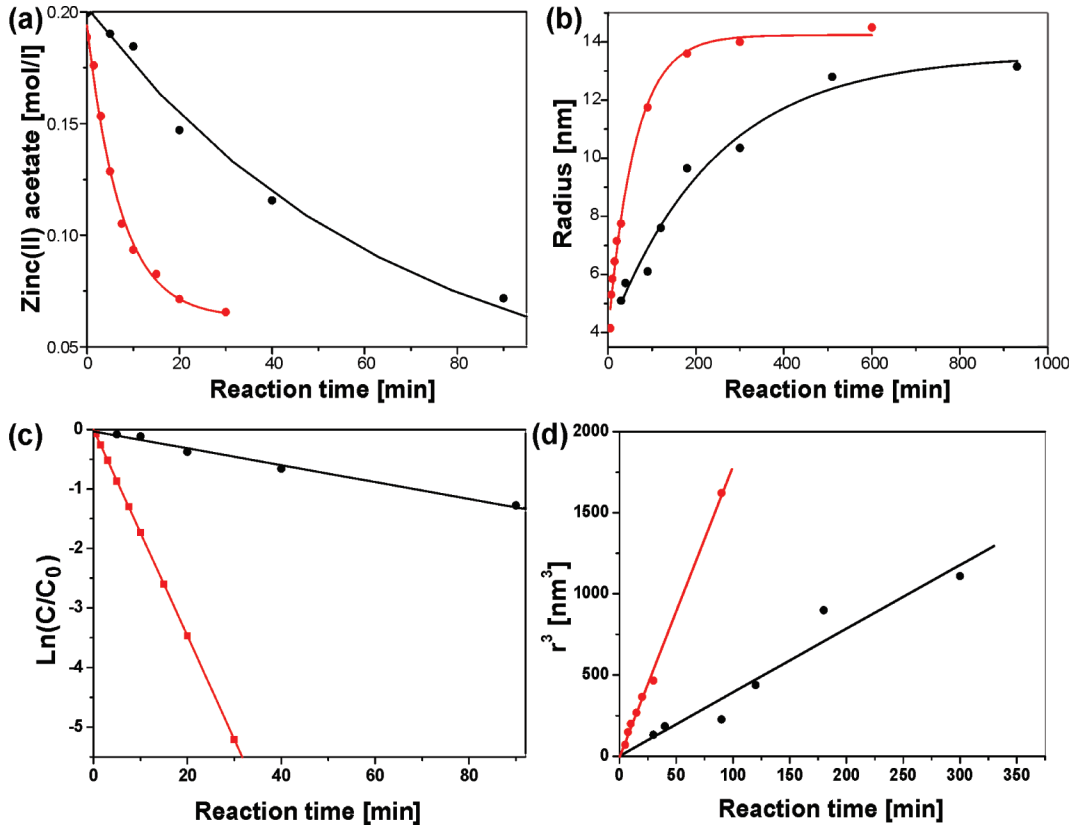

Figure 6. Comparison of benzyl acetate (a, c) and ZnO formation (b, d) using microwave (red) and conventional heating (black) at 120 °C. (a) Zinc acetate concentration *vs* reaction time, (c) corresponding first order kinetic plot. (b) Radius of the ZnO nanocrystals *vs* reaction time, (d) r^3 *vs* time according to the LSW model.

57 kJ/mol).[74] In contrast to that, the same authors presented rate constants in the range of 0.004−0.011 min^{-1} (at 120 °C for different zeolites), which are 1 order of magnitude smaller than $k_{esterification}$ of 0.173 min^{-1} found in this work for the same temperature. On the inorganic side, that is, growth of ZnO, Oskam *et al*. reported an activation energy of 34 kJ mol^{-1} for coarsening of ZnO nanoparticles in the zinc acetate−2-propanol system under basic conditions.[60] This value is considerably lower than the 60 kJ/mol found in here. On the other hand, the rate constants k_{growth} of 0.25−3.2 nm^3/s are much larger in our case than the ones of Oskam *et al*.,[60] which are in the range of 10^{-4}−10^{-2} nm^3/s. But one has to keep in mind that the rate constants are strongly temperature dependent and Oskam *et al*. performed their experiments at much lower temperatures (0−75 °C). Therefore, comparison of our data with literature values is questionable, because of the completely different reaction systems and conditions. A meaningful comparison is only possible within the same system, and this is also the best way to find answers, why microwave-mediated processes are so fast. For this purpose, experiments were carried out in an oil bath preheated at 120 °C (conventional heating) under otherwise similar conditions. The obtained results are summarized in Figure 6. Similar to microwave heating, the dissolution of the precursor represents an important part of the process. Whereas complete solubilization of the precursor is observed in the microwave after 3 min, it takes 15 min in the case of conventional heating. The faster dissolution rate of the precursor clearly contributes to the shorter precipitation time of ZnO under microwave irradiation (5 min) in comparison to conventional heating (30 min). However, microwave irradiation also clearly affects the organic esterification reaction. The change of zinc acetate concentration at 120 °C *versus* time shows a big difference between microwave (red curve) and conventional (black curve) heating (Figure 6a), which consequently leads to rather different rate constants (Figure 6c). For conventional heating, $k_{esterification}$ is 0.0142 min^{-1} (matching well with the zeolite-catalyzed esterification, see above), and for microwave heating it is 0.124 min^{-1}, which corresponds to a kinetic enhancement of almost 1 order of magnitude. Faster esterification also means faster increase in monomer concentration, thus suggesting that nucleation occurs earlier for microwave-heated samples. In addition to the esterification reaction, also the crystal growth is considerably enhanced by microwave heating (Figure 6b). The corresponding rate constants k_{growth}, obtained from LSW analysis, are 15.36 nm^3 min^{-1} for microwave heating and only 3.9 nm^3 min^{-1} for conventional heating (Figure 6d), which means that crystal growth under microwave irradiation is about four times faster. A recent work by Jhung *et al*. on the microwave-mediated synthesis of micro-

porous materials has also shown that microwave irradiation accelerates both the nucleation and growth, however with a more pronounced effect on the nucleation stage.[75]

CONCLUSIONS

The formation of ZnO nanoparticles from zinc acetate and benzyl alcohol proceeds along several consecutive steps that involve organic as well as inorganic reactions. The esterification reaction producing benzyl acetate and the monomeric species on the organic side, and nucleation and growth of ZnO on the inorganic side, represent inseparable and fundamental processes on the way to nanoparticle formation. In this particular case here, the dissolution rate and coarsening effects also contribute greatly to the kinetics of ZnO formation. As a conclusion of our results, we can suggest the following growth model for the formation of ZnO nanoparticles. The esterification reaction is responsible for producing the monomers, presumably zinc hydroxo species. Nucleation of ZnO clusters only occurs when the monomer concentration reaches supersaturation; that is, the organic esterification reaction represents the key step as well as the bottleneck of the nucleation process. And it is exactly this esterification reaction that can greatly be accelerated by microwave irradiation. The fact that the crystal growth follows the LSW theory nearly from the very beginning, and that within the same temperature no sudden change in the growth rate was observed, indicates on the one hand that monomer formation (as a result of the esterification reaction) does not influence the growth rate, and on the other hand, that the growth follows a single growth regime, which is clearly dominated by a constantly ongoing Ostwald ripening. Also the coarsening is greatly affected by microwave irradiation. Liquid−solid interfaces with specific dielectric constants were reported to be sensitive toward local overheating, which improved the mass exchange at the surface, and thus contributed to an increased growth rate.[27,42,43] This statement is supported by the observation that the initial high microwave power rapidly drops once the reaction is initiated (*cf.* Figure 1). In addition to the esterification reaction and the crystal growth, microwave irradiation also accelerates ZnO formation by improving the thermal ramping, resulting in a fast heating of the reaction mixture, and the dissolution of the precursor in benzyl alcohol. Although this aspect was not studied conclusively, our results suggest that the acceleration effect of microwave irradiation is mainly based on kinetic rather than on thermodynamic factors, because no experimental indication was found that the activation energy for ester formation or for crystal growth was significantly lowered. Although our experiments are based on very simple kinetic and thermodynamic models new insights into fundamental and general principles of nanoparticle formation using nonaqueous sol−gel chemistry can be gained, including the role of microwave irradiation on the reaction rates. Although reaction parameters such as precursor−solvent reactivity, precursor concentration, reaction time, and reaction temperature are well-known to influence the size and shape of nanoparticle, these effects can partly be rationalized on the basis of this kinetic study and might contribute to the development of a predictable synthesis planning for metal oxide nanoparticles.

EXPERIMENTAL SECTION

Materials. Zn(II) acetate (99.99%) was used as ZnO precursor and anhydrous benzyl alcohol (99.8%) as solvent. Benzyl acetate (purum, 99.0%) was used for *FTIR* calibration. All the chemicals were purchased from Sigma-Aldrich and used as received.

Synthesis. The typical synthesis of the ZnO nanoparticles was performed by dissolving 1 mmol of zinc acetate in 5 mL of benzyl alcohol in a glovebox under Ar atmosphere (O_2 and $H_2O < 0.1$ ppm). The reaction mixture was transferred into a 10 mL glass tube and sealed with a Teflon cap. During microwave heating, the reaction mixture is stirred with a stir bar. To study the influence of time and temperature in the microwave, the heat treatment was performed in a temperature range of 120−180 °C with irradiation times of 30 s−35 min. The precipitate was separated from the liquid phase by centrifugation, washed with ethanol and diethyl ether, and dried at 60 °C overnight. The powders obtained were weighed to determine the yield, ground in a mortar, and used for the XRD measurments to identify the crystal phase and size. The mother solutions were kept for GC-MS and FTIR measurements. The detailed microwave heating protocol was as follows: During a typical run, the organic reaction is initiated by increasing the power to 300 W and rapidly heating the solution to the required temperature. The reaction temperature is kept constant when the reaction times were changed. The reaction is stopped by thermal quenching by a compressed air flow. The temperature and the pressure are controlled by an IR thermometer and a pressure sensor, respectively.

Instruments and Characterization. The MW experiments were conducted using a CEM Discover reactor operating at a frequency of 2.45 GHz. X-ray powder diffraction studies (XRD) were performed on a Philips PW 1800 diffractometer in reflection mode using a Cu Kα radiation and equipped with a postsample monochromator. Transmission electron microscopy (TEM) and high-resolution transmission electron microscopy were performed on a Philips CM30ST instrument (LaB_6 cathode, operated at 300 kV, point resolution of 2 Å). The samples were ground and then suspended in ethanol. One drop of this suspension was deposited on a 400-mesh carbon-coated copper grid. To minimize agglomeration of the nanoparticles the copper grid was placed on a filter paper. Gas chromatography coupled to mass spectrometry (GC−MS) was performed on a ThermoQuest Trace MS quadrupole instrument equipped with a 60 m × 0.25 mm Zebron ZB-1 ms (Phenomenex) column. Helium was used as carrier gas (flow rate of 0.8 mL/min, split ratio 1:500). The oven temperature was maintained isothermal at 40 °C for 5 min, then increased by 20 °C/min from 50 to 250 °C. The scan rate of the mass spectrometer was 2.5 scans/s over the *m/z* range of 10−300. Fourier transform infrared spectroscopy (FTIR) study of the remaining solutions was done in the wavelength range of 4000−400 cm^{-1} using a Nicolet 5 SXC spectrometer. The spectra were recorded by absorption mode at 4 cm^{-1} interval and 32-times scanning.

The background spectrum was obtained against benzyl alcohol. To get the concentration of benzyl acetate an external calibration curve based on the Lambert−Beer law was obtained by measuring the absorption of benzyl acetate in benzyl alcohol with the concentrations of 0.021, 0.04211, 0.07018, 0.21056, 0.2807, and 0.4211 mol/L.

Acknowledgment. We thank ETH Zürich for financial support, Dr. Igor Djerdj for the TEM and HRTEM measurements, Guido Grassi (Laboratory for Physical Chemistry, ETH Zürich) for the use of the GC−MS facilities, and Prof. Dr. Peter Walde (Institute for Polymers, ETH Zürich) for the use of the IR spectrometer and for helpful discussions.

REFERENCES AND NOTES

1. Burda, C.; Chen, X.; Narayanan, R.; El-Sayed, M. A. Chemistry and Properties of Nanocrystals of Different Shapes. *Chem. Rev.* **2005**, *105*, 1025–1102.
2. Patzke, G. R.; Krumeich, F.; Nesper, R. Oxidic Nanotubes and Nanorods−Anisotropic Modules for a Future Nanotechnology. *Angew. Chem., Int. Ed.* **2002**, *41*, 2446–2461.
3. Jun, Y. W.; Choi, J. S.; Cheon, J. Shape Control of Semiconductor and Metal Oxide Nanocrystals through Nonhydrolytic Colloidal Routes. *Angew. Chem., Int. Ed.* **2006**, *45*, 3414–3439.
4. Park, J.; Joo, J.; Kwon, S. G.; Jang, Y.; Hyeon, T. Synthesis of Monodisperse Spherical Nanocrystals. *Angew. Chem., Int. Ed.* **2007**, *46*, 4630–4660.
5. Garnweitner, G.; Niederberger, M. Organic Chemistry in Inorganic Nanomaterials Synthesis. *J. Mater. Chem.* **2008**, *18*, 1171–1182.
6. Niederberger, M. Nonaqueous Sol-Gel Routes to Metal Oxide Nanoparticles. *Acc. Chem. Res.* **2007**, *40*, 793–800.
7. Pinna, N.; Niederberger, M. Surfactant-Free Nonaqueous Synthesis of Metal Oxide Nanostructures. *Angew. Chem., Int. Ed.* **2008**, *47*, 5292–5304.
8. Mingos, D. M. P. Microwave Syntheses of Inorganic Materials. *Adv. Mater.* **1993**, *5*, 857–859.
9. Rao, K. J.; Vaidhyanathan, B.; Ganguli, M.; Ramakrishnan, P. A. Synthesis of Inorganic Solids using Microwaves. *Chem. Mater.* **1999**, *11*, 882–895.
10. Komarneni, S. Nanophase Materials by Hydrothermal, Microwave-Hydrothermal and Microwave-Solvothermal Methods. *Curr. Sci.* **2003**, *85*, 1730–1734.
11. Shi, S.; Hwang, J.-Y. Microwave-Assisted Wet Chemical Synthesis: Advantages, Significance, and Steps to Industrialization. *J. Miner. Mater. Charact. Eng.* **2003**, *2*, 101–110.
12. Leonelli, C.; Lojkowski, W. Main Development Directions in the Application of Microwave Irradiation to the Synthesis of Nanopowders. *Chem. Today* **2007**, *25*, 34–38.
13. Tsuji, M.; Hashimoto, M.; Nishizawa, Y.; Kubokawa, M.; Tsuji, T. Microwave-Assisted Synthesis of Metallic Nanostructures in Solution. *Chem.—Eur. J.* **2005**, *11*, 440–452.
14. Nadagouda, M. N.; Varma, R. S. Microwave-Assisted Shape-Controlled Bulk Synthesis of Ag and Fe Nanorods in Poly(ethylene glycol) Solutions. *Cryst. Growth Des.* **2008**, *8*, 291–295.
15. Liu, S.-F.; Abothu, I. R.; Komarneni, S. Barium Titanate Ceramics Prepared from Conventional and Microwave Hydrothermal Powders. *Mater. Lett.* **1999**, *38*, 344–350.
16. Wang, W. W.; Zhu, Y. J. Shape-Controlled Synthesis of Zinc Oxide by Microwave Heating Using an Imidazolium Salt. *Inorg. Chem. Commun.* **2004**, 1003–1005.
17. Baldassari, S.; Komarneni, S.; Mariani, E.; Villa, C. Microwave-Hydrothermal Process for the Synthesis of Rutile. *Mater. Res. Bull.* **2005**, *40*, 2014–2020.
18. Murugan, A. V.; Samuel, V.; Ravi, V. Synthesis of Nanocrystalline Anatase TiO_2 by Microwave Hydrothermal Method. *Mater. Lett.* **2006**, *60*, 479–480.
19. Ding, K. L.; Miao, Z. J.; Liu, Z. M.; Zhang, Z. F.; Han, B. X.; An, G. M.; Miao, S. D.; Xie, Y. Facile Synthesis of High Quality TiO_2 Nanocrystals in Ionic Liquid *via* a Microwave-Assisted Process. *J. Am. Chem. Soc.* **2007**, *129*, 6362–6363.
20. Michailovski, A.; Kiebach, R.; Bensch, W.; Grunwaldt, J. D.; Baiker, A.; Komarneni, S.; Patzke, G. R. Morphological and Kinetic Studies on Hexagonal Tungstates. *Chem. Mater.* **2007**, *19*, 185–197.
21. Hu, X. L.; Yu, J. C.; Gong, J. M.; Li, Q.; Li, G. S. Alpha-Fe_2O_3 Nanorings Prepared by a Microwave-Assisted Hydrothermal Process and Their Sensing Properties. *Adv. Mater.* **2007**, *19*, 2324–2329.
22. Godinho, M.; Ribeiro, C.; Longo, E.; Leite, E. R. Influence of Microwave Heating on the Growth of Gadolinium-Doped Cerium Oxide Nanorods. *Cryst. Growth Des.* **2008**, *8*, 384–386.
23. Jouhannaud, J.; Rossignol, J.; Stuerga, D. Rapid Synthesis of Tin (IV) Oxide Nanoparticles by Microwave Induced Thermohydrolysis. *J. Solid State Chem.* **2008**, *181*, 1439–1444.
24. Fidelus, J.; Piticescu, R. R.; Piticescu, R. M.; Lojkowski, W.; Giurgiu, L. Solvothermal Synthesis of Co-Doped ZnO Nanopowders. *Z. Naturforsch., B: Chem. Sci.* **2008**, *63*, 725–729.
25. Hammarberg, E.; Prodi-Schwab, A.; Feldmann, C. Microwave-Assisted Synthesis of Indium Tin Oxide Nanocrystals in Polyol Media and Transparent, Conductive Layers thereof. *Thin Solid Films* **2008**, *516*, 7437–7442.
26. Zhu, P. L.; Zhang, J. W.; Wu, Z. S.; Zhang, Z. J. Microwave-Assisted Synthesis of Various ZnO Hierarchical Nanostructures: Effects of Heating Parameters of Microwave Oven. *Cryst. Growth Des.* **2008**, *8*, 3148–3153.
27. Hu, X.; Gong, J.; Zhang, L.; Yu, J. C. Continuous Size Tuning of Monodisperse ZnO Colloidal Nanocrystal Clusters by a Microwave-Polyol Process and Their Application for Humidity Sensing. *Adv. Mater.* **2008**, *20*, 4845–4850.
28. Nyutu, E. K.; Chen, C. H.; Dutta, P. K.; Suib, S. L. Effect of Microwave Frequency on Hydrothermal Synthesis of Nanocrystalline Tetragonal Barium Titanate. *J. Phys. Chem. C* **2008**, *112*, 9659–9667.
29. Kerner, R.; Palchik, O.; Gedanken, A. Sonochemical and Microwave-Assisted Preparations of PbTe and PbSe. A Comparative Study. *Chem. Mater.* **2001**, *13*, 1413–1419.
30. Murugan, A. V.; Sonawane, R. S.; Kale, B. B.; Apte, S. K.; Kulkarni, A. V. Microwave-Solvothermal Synthesis of Nanocrystalline Cadmium Sulfide. *Mater. Chem. Phys.* **2001**, *71*, 98–102.
31. Gerbec, J. A.; Magana, D.; Washington, A.; Strouse, G. F. Microwave-Enhanced Reaction Rates for Nanoparticle Synthesis. *J. Am. Chem. Soc.* **2005**, *127*, 15791–15800.
32. Li, L.; Qian, H. F.; Ren, J. Rapid Synthesis of Highly Luminescent CdTe Nanocrystals in the Aqueous Phase by Microwave Irradiation with Controllable Temperature. *Chem. Commun.* **2005**, 528–530.
33. Jiang, Y.; Zhu, Y. J. Microwave-Assisted Synthesis of Sulfide M_2S_3 (M = Bi, Sb) Nanorods Using an Ionic Liquid. *J. Phys. Chem. B* **2005**, *109*, 4361–4364.
34. Qian, H. F.; Qiu, X.; Li, L.; Ren, J. C. Microwave-Assisted Aqueous Synthesis: A Rapid Approach to Prepare Highly Luminescent ZnSe(S) Alloyed Quantum Dots. *J. Phys. Chem. B* **2006**, *110*, 9034–9040.
35. Panda, A. B.; Glaspell, G.; El-Shall, M. S. Microwave Synthesis of Highly Aligned Ultra Narrow Semiconductor Rods and Wires. *J. Am. Chem. Soc.* **2006**, *128*, 2790–2791.
36. He, Y.; Sai, L. M.; Lu, H. T.; Hu, M.; Lai, W. Y.; Fan, Q. L.; Wang, L. H.; Huang, W. Microwave-Assisted Synthesis of Water-Dispersed CdTe Nanocrystals with High Luminescent Efficiency and Narrow Size Distribution. *Chem. Mater.* **2007**, *19*, 359–365.
37. Ziegler, J.; Merkulov, A.; Grabolle, M.; Resch-Genger, U.; Nann, T. High-Quality ZnS Shells for CdSe Nanoparticles: Rapid Microwave Synthesis. *Langmuir* **2007**, *23*, 7751–7759.

38. Bühler, G.; Feldmann, C. Microwave-Assisted Synthesis of Luminescent $LaPO_4$:Ce, Tb Nanocrystals in Ionic Liquids. *Angew. Chem., Int. Ed.* **2006**, *45*, 4864–4867.
39. Murugan, A. V.; Muraliganth, T.; Manthiram, A. Comparison of Microwave Assisted Solvothermal and Hydrothermal Syntheses of $LiFePO_4$/C Nanocomposite Cathodes for Lithium Ion Batteries. *J. Phys. Chem. C* **2008**, *112*, 14665–14671.
40. Bose, A. K.; Manhas, M. S.; Banik, B. K.; Robb, E. W. Microwave-Induced Organic Reaction Enhancement (MORE) Chemistry: Techniques for Rapid, Safe and Inexpensive Synthesis. *Res. Chem. Intermed.* **1994**, *20*, 1–11.
41. Kappe, C. O. Controlled Microwave Heating in Modern Organic Synthesis. *Angew. Chem., Int. Ed.* **2004**, *43*, 6250–6284.
42. Conner, W. C.; Tompsett, G. A. How Could and Do Microwaves Influence Chemistry at Interfaces. *J. Phys. Chem. B* **2008**, *112*, 2110–2118.
43. Vallee, S. J.; Conner, W. C. Microwaves and Sorption on Oxides: A Surface Temperature Investigation. *J. Phys. Chem. B* **2006**, *110*, 15459–15470.
44. Niederberger, M.; Garnweitner, G. Organic Reaction Pathways in the Nonaqueous Synthesis of Metal Oxide Nanoparticles. *Chem.—Eur. J.* **2006**, *12*, 7282–7302.
45. Bilecka, I.; Djerdj, I.; Niederberger, M. One-Minute Synthesis of Crystalline Binary and Ternary Metal Oxide Nanoparticles. *Chem. Commun.* **2008**, 886–888.
46. La Mer, V. K.; Dinegar, R. H. Theory, Production and Mechanism of Formation of Monodispersed Hydrosols. *J. Am. Chem. Soc.* **1950**, *72*, 4847–4854.
47. La Mer, V. K. Nucleation in Phase Transitions. *Ind. Eng. Chem.* **1952**, *44*, 1270–1277.
48. Reiss, H. The Growth of Uniform Colloidal Dispersions. *J. Chem. Phys.* **1951**, *19*, 482–487.
49. Nielsen, A. E. Nucleation and Growth of Crystals at High Supersaturation. *Kristall. Technol.* **1969**, *4*, 17–38.
50. Sugimoto, T. Preparation of Monodispersed Colloidal Particles. *Adv. Colloid Interface Sci.* **1987**, *28*, 65–108.
51. Talapin, D. V.; Rogach, A. L.; Haase, M.; Weller, H. Evolution of an Ensemble of Nanoparticles in a Colloidal Solution: Theoretical Study. *J. Phys. Chem. B* **2001**, *105*, 12278–12285.
52. Barnard, A. S.; Curtiss, L. A. Prediction of TiO_2 Nanoparticle Phase and Shape Transitions Controlled by Surface Chemistry. *Nano Lett.* **2005**, *5*, 1261–1266.
53. Ba, J.; Feldhoff, A.; Fattakhova Rohlfing, D.; Wark, M.; Antonietti, M.; Niederberger, M. Crystallization of Indium Tin Oxide Nanoparticles: From Cooperative Behavior to Individuality. *Small* **2007**, *3*, 310–317.
54. Yang, C. S.; Awschalom, D. D.; Stucky, G. D. Kinetic-Dependent Crystal Growth of Size-Tunable CdS Nanoparticles. *Chem. Mater.* **2001**, *13*, 594–598.
55. Piepenbrock, M. O. M.; Stirner, T.; O'Neill, M.; Kelly, S. M. Growth Dynamics of CdTe Nanoparticles in Liquid and Crystalline Phases. *J. Am. Chem. Soc.* **2007**, *129*, 7674–7679.
56. Peng, X. G.; Wickham, J.; Alivisatos, A. P. Kinetics of II-VI and III-V Colloidal Semiconductor Nanocrystal Growth: "Focusing" of Size Distributions. *J. Am. Chem. Soc.* **1998**, *120*, 5343–5344.
57. Kwon, S. G.; Piao, Y.; Park, J.; Angappane, S.; Jo, Y.; Hwang, N. M.; Park, J. G.; Hyeon, T. Kinetics of Monodisperse Iron Oxide Nanocrystal Formation by "Heating-up" Process. *J. Am. Chem. Soc.* **2007**, *129*, 12571–12584.
58. Wong, E. M.; Bonevich, J. E.; Searson, P. C. Growth Kinetics of Nanocrystalline ZnO Particles from Colloidal Suspensions. *J. Phys. Chem. B* **1998**, *102*, 7770–7775.
59. Wong, E. M.; Hoertz, P. G.; Liang, C. J.; Shi, B. M.; Meyer, G. J.; Searson, P. C. Influence of Organic Capping Ligands on the Growth Kinetics of ZnO Nanoparticles. *Langmuir* **2001**, *17*, 8362–8367.
60. Oskam, G.; Hu, Z. S.; Penn, R. L.; Pesika, N.; Searson, P. C. Coarsening of Metal Oxide Nanoparticles. *Phys. Rev. E* **2002**, *66*, 011403.
61. Hu, Z. S.; Oskam, G.; Searson, P. C. Influence of Solvent on the Growth of ZnO Nanoparticles. *J. Colloids Interface Sci.* **2003**, *263*, 454–460.
62. Hu, Z. S.; Santos, J. F. H.; Oskam, G.; Searson, P. C. Influence of the Reactant Concentrations on the Synthesis of ZnO Nanoparticles. *J. Colloids Interface Sci.* **2005**, *288*, 313–316.
63. Li, W. J.; Shi, E. W.; Zhong, W. Z.; Yin, Z. W. Growth Mechanism and Growth Habit of Oxide Crystals. *J. Cryst. Growth* **1999**, *203*, 186–196.
64. Taubert, A.; Glasser, G.; Palms, D. Kinetics and Particle Formation Mechanism of Zinc Oxide Particles in Polymer-Controlled Precipitation from Aqueous Solution. *Langmuir* **2002**, *18*, 4488–4494.
65. Michailovski, A.; Grunwaldt, J. D.; Baiker, A.; Kiebach, R.; Bensch, W.; Patzke, G. R. Studying the Solvothermal Formation of MoO_3 Fibers by Complementary *in-situ* EXAFS/EDXRD Techniques. *Angew. Chem., Int. Ed.* **2005**, *44*, 5643–5647.
66. Oskam, G.; Nellore, A.; Penn, R. L.; Searson, P. C. The Growth Kinetics of TiO_2 Nanoparticles from Titanium(IV) Alkoxide at High Water/Titanium Ratio. *J. Phys. Chem. B* **2003**, *107*, 1734–1738.
67. Lee, E. J. H.; Ribeiro, C.; Longo, E.; Leite, E. R. Growth Kinetics of Tin Oxide Nanocrystals in Colloidal Suspensions under Hydrothermal Conditions. *Chem. Phys.* **2006**, *328*, 229–235.
68. Wagner, C. Theorie der Alterung von Niederschlägen durch Umlösen (Ostwald-Reifung). *Z. Elektrochem.* **1961**, *65*, 581–591.
69. Lifshitz, I. M.; Slyozov, V. V. The Kinetics of Precipitation from Supersaturated Solid Solutions. *J. Phys. Chem. Solids* **1961**, *19*, 35–50.
70. Ardell, A. J. Effect of Volume Fraction on Particle Coarsening—Theoretical Considerations. *Acta Metallurg.* **1972**, *20*, 61–71.
71. Baldan, A. Progress in Ostwald Ripening Theories and Their Applications to Nickel-Base Superalloys. *J. Mater. Sci.* **2002**, *37*, 2171–2202.
72. Clavel, G.; Willinger, M. G.; Zitoun, D.; Pinna, N. Solvent Dependent Shape and Magnetic Properties of Doped ZnO Nanostructures. *Adv. Funct. Mater.* **2007**, *17*, 3159–3169.
73. Hayakawa, S.; Matsui, T.; Tanaka, S. FT-IR Study of Ester Solubilization into a Micelle Solution. *Appl. Spectrosc.* **1987**, *41*, 1438–1441.
74. Kirumakki, S. R.; Nagaraju, N.; Narayanan, S. A Comparative Esterification of Benzyl Alcohol with Acetic Acid over Zeolites Hβ, HY, and HZSM5. *Appl. Catal., A* **2004**, *273*, 1–9.
75. Jhung, S. H.; Jin, T. H.; Hwang, Y. K.; Chang, J. S. Microwave Effect in the Fast Synthesis of Microporous Materials: Which Stage Between Nucleation and Crystal Growth is Accelerated by Microwave Irradiation. *Chem.—Eur. J.* **2007**, *13*, 4410–4417.